Spatiotemporal scaling of hydrological and agrochemical export dynamics in a tile-drained Midwestern watershed

K. Guan,[1] S. E. Thompson,[2,3] C. J. Harman,[4] N. B. Basu,[5] P. S. C. Rao,[6] M. Sivapalan,[4,7,8] A. I. Packman,[9] and P. K. Kalita[10]

Received 10 September 2010; revised 17 January 2011; accepted 10 February 2011; published 11 May 2011.

[1] Conceptualizing catchments as physicochemical filters is an appealing way to link streamflow discharge and concentration time series to hydrological and biogeochemical processing in hillslopes and drainage networks. Making these links explicit is challenging in complex watersheds but may be possible in highly modified catchments where hydrological and biogeochemical processes are simplified. Linking hydrological and biogeochemical filtering in highly modified watersheds is appealing from a water quality perspective in order to identify the major controls on chemical export at different spatial and temporal scales. This study investigates filtering using a 10 year data set of hydrological and biogeochemical export from a small (<500 km^2) agricultural watershed in Illinois, the Little Vermilion River (LVR) Watershed. A number of distinct scaling regimes were identified in the Fourier power spectrum of discharge and nitrate, phosphate, and atrazine concentrations. These scaling regimes were related to different runoff pathways and spatial scales throughout the catchment (surface drainage, tile drains, and channel flow in the river). Wavelet analysis indicated increased coupling between discharge and in-stream concentrations at seasonal-annual time scales. Using a multiresolution analysis, nitrate, phosphate, and atrazine loads exported at annual scales were found to exhibit near-linear scaling with annual streamflow, suggesting that at these scales the export dynamics could be approximated as chemostatic responses. This behavior was pronounced for nitrate and less so for phosphate and atrazine. The analysis suggests that biogeochemical inputs built up legacy loads, leading to the emergence of chemostatic behavior at annual time scales, even at the relatively small scale of the LVR.

Citation: Guan, K., S. E. Thompson, C. J. Harman, N. B. Basu, P. S. C. Rao, M. Sivapalan, A. I. Packman, and P. K. Kalita (2011), Spatiotemporal scaling of hydrological and agrochemical export dynamics in a tile-drained Midwestern watershed, *Water Resour. Res.*, *47*, W00J02, doi:10.1029/2010WR009997.

1. Introduction: Catchments as Physicochemical Filters

[2] The conceptualization of hydrological systems as a cascade of hierarchical filters, transforming an input signal of rainfall [*Matsoukas et al.*, 2000] through infiltration [*Meng et al.*, 2006] and the water table [*Li and Zhang*, 2007] to produce a streamflow response [*Sauquet et al.*, 2008], has a growing history in statistical hydrology [*Tessier et al.*, 1996]. This area of study has focused on the time series features of hydrological signatures, in particular with respect to their multifractal properties, the emergence of multiple scaling regimes, and the consequences for prediction of extreme events [*Schertzer et al.*, 2006]. Rainfall drives the generation of hydrological responses in catchments, so it is reasonable to expect that the resulting hydrological signatures should inherit the scaling properties of rainfall, smoothed to varying extents depending upon filtering due to soil water deficits induced by evapotranspiration losses, and the resulting distribution of residence times in the system [*Zhou et al.*, 2006]. This smoothing can be isolated (in some cases) as the transfer function that converts the input signature into an output, and this transfer function represents

[1]Department of Civil and Environmental Engineering, Princeton University, Princeton, New Jersey, USA.
[2]School of Civil and Environmental Engineering, Purdue University, West Lafayette, Indiana, USA.
[3]Now at Nicholas School of the Environment, Duke University, Durham, North Carolina, USA.
[4]Department of Civil and Environmental Engineering, University of Illinois at Urbana-Champaign, Urbana, Illinois, USA.
[5]Department of Civil Engineering, University of Iowa, Iowa City, Iowa, USA.
[6]School of Civil and Environmental Engineering, Purdue University, West Lafayette, Indiana, USA.
[7]Department of Geography, University of Illinois at Urbana-Champaign, Urbana, Illinois, USA.
[8]Department of Water Management, Delft University of Technology, Delft, Netherlands.
[9]Department of Civil Engineering, Northwestern University, Evanston, Illinois, USA.
[10]Department of Agriculture and Biological Engineering, University of Illinois at Urbana-Champaign, Urbana, Illinois, USA.

0043-1397/11/2010WR009997

the hydrological filtering action of the catchment [*Schertzer et al.*, 2006]. However, a unique transfer function approach may not always be applicable, especially in highly transient systems where catchment residence time distributions are time variant [*Majone et al.*, 2010].

[3] Treating catchments as hydrological filters offers an alternative conceptualization to either detailed, distributed process modeling or lumped, whole-catchment "black box" models. The body of existing studies on catchments as filters, however, could be extended in two significant ways. First, the properties of filtering in the catchment could be linked more explicitly to the underlying mechanistic processes of rainfall-runoff response [*Kirchner*, 2009]. Second, hydrological fluxes drive many other critical functions of watersheds, including biogeochemical processing, ecological functioning, and the utility of ecosystems for human exploitation.

[4] While the role of a catchment as a hydrologic filter has been relatively well explored in different contexts, biogeochemical "filtering" as driven by the catchment hydrology has only recently begun to receive equal attention, in part because of the difficulties associated with collecting high-resolution time series of export over sufficiently long periods of time [*Kirchner et al.*, 2004; *Godsey et al.*, 2010]. Much of the interest in understanding the temporal scaling of solute concentrations has been driven by studies of conservative tracers, which can offer insight into travel time distributions of water in the catchment [*Kirchner et al.*, 2000, 2001; *Godsey et al.*, 2010]. Spectral techniques have been used to infer retardation constants for atmospherically derived tracers [*Feng et al.*, 2004a] and to explore the signatures of nitrogen transport [*Zhang and Schilling*, 2005]. Broader questions relating to the interplay of biogeochemical reactivity, biological uptake and release, retardation processes, and transport pathways as drivers of catchment biogeochemistry and their reflection in the scaling properties of stream biogeochemistry largely remain to be addressed. A combination of field studies and simulations suggests that processes occurring within shallow saturated zones [*Zhang and Schilling*, 2004], karstic or fractured aquifers [*Majone et al.*, 2004], hyporheic zones [*Cardenas*, 2008], and the vadose zone [*Feng et al.*, 2004a] can all contribute to observed power law scaling of biogeochemical export and in-stream concentrations. Given the potential complexity of both hydrological [*Botter et al.*, 2010] and biogeochemical filtering processes, inference linking filtering to physicochemical mechanisms is most feasible in catchments with simple hydrology. Even in relatively simple systems, it has been argued that explicit observation of individual flow paths is needed to make reasonable predictions about solute transport [*Rozemeijer et al.*, 2010a].

[5] The tile-drained watersheds of the Midwestern United States present ideal examples of such simplified catchments. Contemporary Midwestern landscapes are essentially human creations, reflecting an almost complete conversion of natural prairies, wetlands, and forests to croplands. Vast tracts of land (~75% or approximately a 500,000 km^2 area) are planted to corn-soybean rotation. The hydrology of the Midwestern landscapes has been extensively modified to promote rapid drainage, primarily by the construction of extensive networks of artificial drainage (surface ditches and subsurface tile drains) [*Basu et al.*, 2010a; *Schilling and Helmers*, 2008]. The artificial drainage network increases the hydrological connectivity of the landscape to the channels, allowing flows to bypass much of the complexity of the landscape. This promotes spatial homogeneity in runoff generation, leading to flashy responses to rainfall and exponential recession curves which dominate flow in the artificial drainage network and the streams [*Evans and Fausey*, 1999; *Basu et al.*, 2010a]. Further, in these watersheds, the application of fertilizers, pesticides, and animal manures has significantly perturbed the natural biogeochemical regime. The application of agrochemicals has impacted water quality at both the local scale, across the basin as a whole, and in receiving water bodies, most dramatically in driving coastal hypoxia in the Gulf of Mexico [*Rabalais et al.*, 2002; *Phillips et al.*, 2006; *Blann et al.*, 2009; *McLaughlin and Mineau*, 1995].

[6] The water quality impacts of agricultural drainage are driven by the exported chemical mass load (L), typically computed as the product of concentration (C) and the discharge rate (Q). Variation and covariation of C and Q are both important controls on the dynamics of L [*Borsuk et al.*, 2004]. In a recent analysis of agricultural watersheds from around the world, *Basu et al.* [2010b] demonstrated that loads of total nitrogen and total phosphorus were well approximated as a linear function of Q at large spatial scales and annual time scales. This implies that the annually flow-weighted value of C was essentially constant, a phenomenon we will refer to here as "chemostatic behavior." For smaller, unmanaged catchments, and at all time scales, *Godsey et al.* [2009] showed that chemostatic behavior provided an excellent description of the export dynamics of a range of geologically derived solutes. *Basu et al.* [2010b] hypothesized that the chemostatic behavior of nutrients in large basins arose from legacy effects, namely, the large accumulated stores of N and P in agricultural landscapes. As a result, these anthropogenic compounds behaved analogously to geologically derived species such as calcium or magnesium salts. A secondary question motivating the study of hydrological and biogeochemical filtering in agricultural watersheds, then, is to ascertain the spatiotemporal scale dependence of chemostatic behavior and the possible determinants of such dependence.

[7] Of course, despite the simplicity of an agricultural catchment in comparison to unmanaged catchments, the catchments are nonetheless dynamic, and much of the dynamism is driven by intensive management practices and seasonal cycles of crop planting, growth, and harvest. For example, crop growth cycles have an important effect on the seasonal changes in the uptake of water and nutrients from the root zone, as influenced by the changes over time in the depth distribution of roots and the maximum rooting depth. Thus, the crop-available amount of water and nutrients increases from late spring through the summer growing season, as the root zone increases. Crop uptake represents a large sink for both water and nutrients, and the periodicity of this uptake is anticipated to contribute to the function of the catchment as a filter.

[8] In this study, we investigate the spatiotemporal variation and covariation of C, Q, and L for three agrochemicals: nitrate (NO_3^-), phosphate (PO_4^{3-}), and atrazine. The study analyzes these dynamics within a small (<500 km^2) agricultural watershed in eastern Illinois, the Little Vermilion River (LVR) Watershed, which exhibits the simplifying features (dense artificial drainage networks, relatively

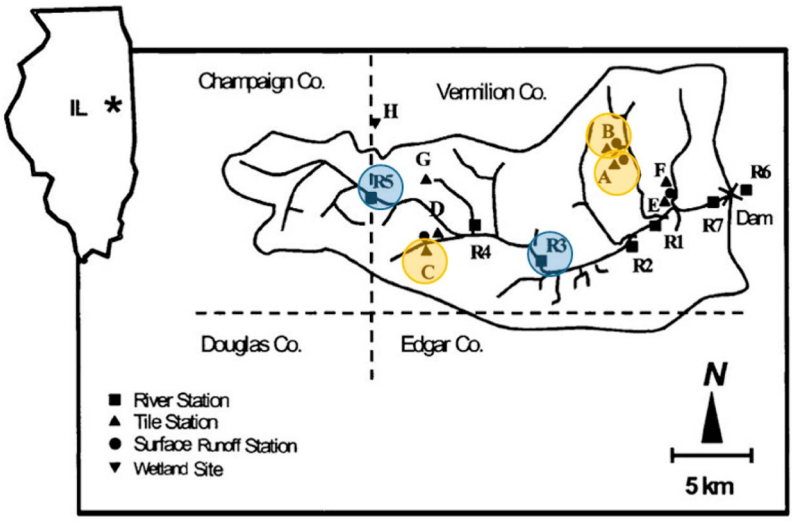

Figure 1. The Little Vermilion River Watershed (LVR), Illinois, United States (40°06′21.45″N, 87°41′34.12″W). The focus of the study is on three colocated tile and surface drainage stations (denoted A_1/A_2, B_1/B_2, and C_1/C_2, where 1 indicates a subsurface tile drain and 2 indicates a surface drain) and two river gauges (R_3 and R_5).

homogeneous cropping, and anthropogenic chemical loading) typical of Midwestern landscapes. The three agrochemicals display different chemical properties in terms of both reactivity and sorption, allowing the effects of these properties on the emergent filtering to be examined together. The study aims to address three guiding questions.

[9] 1. What are the characteristics of the hydrological and biogeochemical filters operating in the LVR?

[10] 2. Can the properties of these filters be used to "fingerprint" different reactive transport processes?

[11] 3. On what spatial and temporal scales are chemostatic responses observed?

[12] These questions are largely addressed through a series of analyses in the frequency domain, documented in section 2. Frequency domain analysis is naturally motivated by the filtering concept, which deconvolves the action of different linear filters, simplifying the analysis. Scaling features that are difficult to distinguish in the time domain are exaggerated in the frequency domain, facilitating comparisons across different sites, scales, and solutes [*Godsey et al.*, 2010]. Finally, frequency domain techniques allow the variability and correlation behavior of time series to be compared and isolated at different temporal scales, making them well suited to an examination of the temporal dependence of chemostatic behavior. The conceptual understanding obtained by addressing the research questions is ultimately synthesized to generate a conceptual model of solute filtering by the landscape of the Little Vermilion River Watershed.

2. Methods

2.1. Study Location and Data Collection

[13] The Little Vermilion River (LVR) Watershed (see Figure 1 for a map), is located in eastern Illinois, United States (40°06′21.45″N, 87°41′34.12″W) [*Mitchell et al.*, 2000]. The LVR watershed has a drainage area of about 489 km^2, generally flat topography with slopes <1°, and primarily silty or silty clay loam soils. Approximately 90% of the watershed is devoted to intensive agricultural production and is cropped under a corn-soybean rotation, typical of many Midwestern agricultural watersheds [*Algoazany*, 2006]. Mean annual precipitation is approximately 1040 mm [*Algoazany*, 2006]. The hydrology in the watershed has been highly modified by the construction of an extensive network of irregularly-spaced subsurface tile drains and surface drainage ditches, which discharge to stream channels. Subsurface drainage dominates the water budget because of the flat topography, with surface runoff being important only during infrequent high-intensity events during early spring when the soil water content is at its maximum [*Mitchell et al.*, 2000]. On average, subsurface runoff represents more than 90% of the total flow. The dominance of the tile drains is also reflected in the chemical export, at least for nitrate and atrazine, 99.5% and 96% of which, respectively, are exported via this pathway. Phosphate, however, is disproportionately represented in the surface flow paths, which accounted for between 28% and 58% of export in the drainage areas studied [*Algoazany*, 2006]. This partitioning is attributable to strong phosphate sorption on fine particulate matter which is readily exported during surface runoff events.

[14] The data used in this study are from a 10 year (1991–2000) project monitoring hydrological variability and water quality in the LVR [*Algoazany*, 2006]. Hydrological fluxes (rainfall and stream flow) were recorded continuously, with flow sampling occurring at 15 min intervals [*Mitchell et al.*, 2000]. Chemical constituents, including nitrate, phosphate, and a number of pesticides were recorded using a stratified sampling design. During low-flow periods chemical sampling was undertaken every 14 days. Above a site-specific flow threshold (summarized in Table 1) higher-frequency sampling (typically at 5 h intervals) was undertaken. Loads were computed by interpolating concentration data between measurements and using the high-frequency flow data. The

Table 1. Monitoring Stations Within the Little Vermilion Watershed That Will Be Used in This Study

Site	Station	Flow Type	Drainage Area (m^2)	Record Coverage	Q Threshold[a] (m^3/s)
A	A1	subsurface (tile)	4.9×10^4	19 Nov 1991 to 31 Dec 2000	10^{-4} m^3/s
	A2	surface	6.0×10^4	20 Jan 1993 to 31 Dec 2000	10^{-4} m^3/s
B	B1	subsurface (tile)	3.3×10^4	20 Nov 1991 to 31 Dec 2000	10^{-4} m^3/s
	B2	surface	3.0×10^4	24 Jul 1993 to 31 Dec 2000	10^{-4} m^3/s
C	C1	subsurface (tile)	6.8×10^4	7 Nov 1992 to 31 Dec 2000	10^{-4} m^3/s
	C2	surface	1.5×10^4	11 Nov 1993 to 31 Dec 2000	10^{-4} m^3/s
R3	R3	river	1.9×10^8	12 Jul 1993 to 31 Dec 2000	10^{-2} m^3/s
R5	R5	river	6.9×10^7	14 Aug 1992 to 31 Dec 2000	10^{-2} m^3/s

[a] Q threshold indicates the minimum flow at which high-frequency monitoring was initiated.

load data were linearly interpolated to give a daily load time series, which was used for the frequency analysis. Although *Rozemeijer et al.* [2010b] found that using sparse concentration data could lead to significant errors in computed loads, this estimate was based on a weekly sampling regime. By contrast, the higher-frequency within-storm sampling undertaken at the Little Vermillion River allows for several concentration measurements to be made during significant storm events, avoiding the gross biases found by *Rozemeijer et al.* [2010b]. Measurement techniques are described by *Algoazany* [2006]. Measurements were taken at a range of spatial scales (local tile drainage areas and several points in the main river channel) so that the contributing areas sampled span 3 orders of magnitude (see Table 1). Each of the local drainage areas had two monitoring stations, one for the tile drain and the other for the surface drains. This study focuses on three colocated tile and surface drainage stations (denoted A_1/A_2, B_1/B_2, and C_1/C_2, where 1 indicates a subsurface tile drain and 2 indicates a surface drain), and two river gauges (R_3 and R_5). Note that the R_5 station is located in the upper catchment and has a smaller drainage area than R_3 (see Figure 1). Detailed data on the timing of agricultural management practices (e.g., fertilizer and herbicide application) were collected for the area around tile flow stations A_1 and B_1 in order to investigate the influence of land management on chemical transport at small scales [*Algoazany*, 2006].

2.2. Biogeochemistry of Nitrate, Phosphate, and Atrazine

[15] In the LVR, the patterns of chemical concentration observed in streamflow can be conceptualized as arising from an interplay between processes that remove chemicals from transport in flow and processes that renew the availability of the solutes for such transport. Renewal processes include natural biogeochemical cycling (weathering, nitrification, etc.) but are dominated by the application of fertilizers and pesticides. Removal from transport may occur because of several different processes, including reversible transformation (e.g., complexation or mineralization), irreversible transformations (e.g., denitrification and volatilization), plant or microbial uptake, or sorption onto soil or colloidal particles. In general, we may characterize the reactivity of species by a reaction constant or, equivalently for first-order reactions, a half-life. Sorption of different chemicals is represented by an effective sorption coefficient, $K_d(L^3/M)$: admittedly, this is a simplification of much more complex models for sorption dynamics [*Brusseau and Rao*, 1989], particularly in the case of phosphate. The chemicals considered here each have different biological, physical, and chemical pathways that remove them from being available for aqueous transport. Simplified reaction formulations are useful because they allow cross comparison of the overall behavior of disparate chemicals during the period of observation.

[16] Of the three solutes analyzed in this paper, nitrate is not significantly sorbed ($K_d \sim 0$), atrazine is weakly sorbing (K_{oc} = 100 L/kg or $K_d \sim 1$ L/kg for soils with 1%–2% organic content [*Wauchope et al.*, 1992]) and phosphorous strongly sorbed ($K_d \sim 330$–5150 L/kg [*Machesky et al.*, 2010]). The phosphorus species analyzed in the LVR is soluble, dissolved inorganic P (PO_4^{3-}). However, phosphate in the aqueous phase is in equilibrium with the sorbed phases (particulate P). We thus expect the phosphate export dynamics to reflect the dynamics of particulate P to a large extent. Soluble atrazine dynamics may weakly reflect the transport of bound atrazine, and nitrate dynamics should be essentially independent of particle movement. The potential for particle-bound transport to be important for strongly sorbing species may have significant implications for the dominant transport processes both on the soil surface and in the vadose zone, with fast flow pathways (overland or preferential flow in macropores or cracks) representing an increased fraction of the export for highly sorbing species [*McGrath*, 2007]. The reactivity of the solutes determines to first order how long the solute can persist in the catchment in the absence of transport. Atrazine has a documented half life of ~60 days [*Wauchope et al.*, 1992]. Reactivity is difficult to estimate for N and P because of internal cycling in association with microbiological and plant uptake. The potential for sorptive, uptake, and reactive processes to result in relatively short lived signals of export in the stream following application to the landscape drives the choice of renewal and removal from transport as the most general descriptors of chemical processing.

2.3. Load Discharge and Concentration Discharge Relationships

[17] Several data analysis techniques were employed to explore the relationships between concentration (C), discharge (Q), and the exported mass loads (L). The initial analysis consisted of comparing the spectral properties of discharge and the exported concentration in the Fourier domain. Wavelet analysis was used to compute the wavelet coherence for the L-Q and Q-C signals. Finally, a multiresolution analysis was used to filter the time series and allow L-Q relationships to be investigated as a function of different averaging windows in the time domain. The

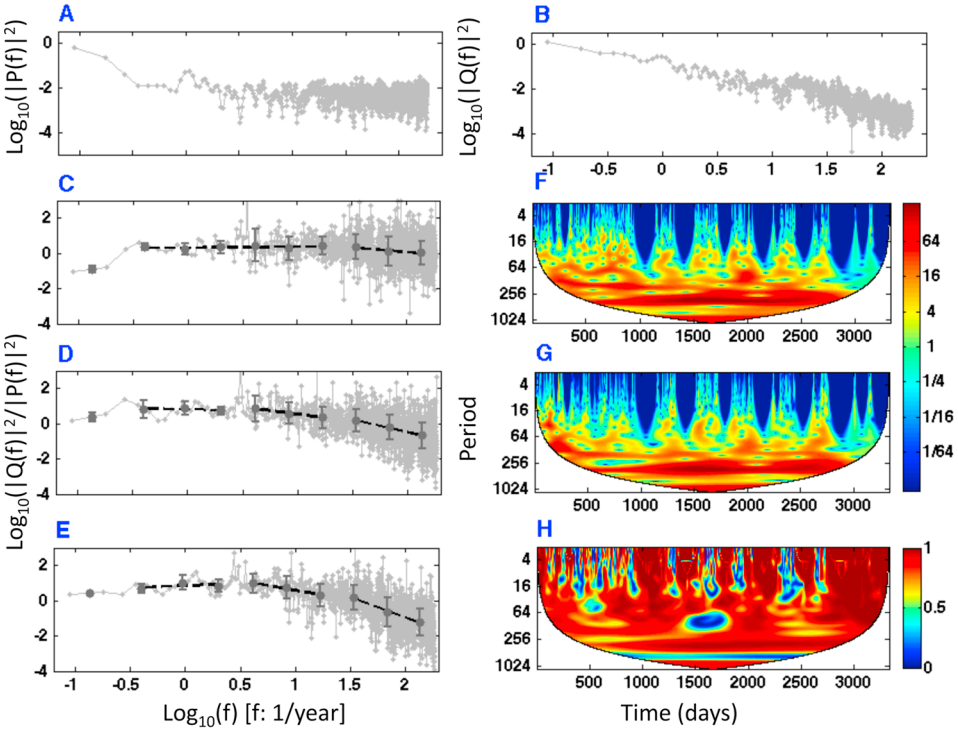

Figure 2. Examples of the power spectra of (a) precipitation and (b) flow at the upper catchment river station R_5 as a function of frequency (f). The ratio of normalized power spectra (with octave binning) of flow and precipitation as a function of frequency (f) for the three sampling station types: (c) surface flow station, (d) tile flow station, and (e) river channel station. Dots show the octave binned values. Error bars indicate the standard deviation within each bin. All power spectra are normalized by the variance (σ^2) of the original time series. Examples of continuous wavelet power spectra of standardized time series of (f) flow and (g) nitrate concentration for the tile drain station B_1. (h) The squared wavelet coherence between the standardized flow and nitrate concentration time series. White regions correspond to the cone of influence (COI) of edge effects.

remainder of this section elaborates on the implementation of these techniques.

2.3.1. Fourier Spectral Analysis

[18] Fourier analysis begins with transforming a time series $X(t)$ from the time (t) domain into the frequency (f) (see equation (1)). The transformed time series are most conveniently viewed in terms of their power spectrum ($|X(f)|^2$) (normalized to have variance equal to 1), which shows how the variance of the time series is partitioned amongst different frequencies [*Katul et al.*, 2007]. Peaks in the power spectrum are indicative of strongly periodic signals in the time series. Flat regions in the power spectrum are referred to as "white noise," in which variability occurs equivalently on all time scales. When the power spectrum is viewed on a log-log scale, linear regions often appear, indicating power law scaling across a range of frequencies, i.e., $|X(f)|^2 \sim f^{-\alpha}$ [*Harris et al.*, 1997]. The slope of such linear regions is often related to processes that induce statistically self-similar behavior [*Fraedrich and Larnder*, 1993]. Usually, such scaling behavior is restricted to a range of frequencies, corresponding to the scales over which the self-similar processes operate (Figures 2a and 2b).

[19] We examined scaling behavior in flow at different sites in the LVR to investigate hydrological filtering (i.e., transformation of rainfall signals into discharge) in the watershed. To isolate the effect of this filtering, we normalized the power spectrum of flow by that of the rainfall. Estimation of the exponent α for different power law regimes and of the breaks in scaling between these regimes is complicated by the fact that power spectra are typically noisy. To avoid errors in fitting due to this noise, we used an octave binning algorithm as a smoothing technique to allow a robust fit. Unlike the traditional window smoothing method, which may result in heavily biased scaling exponent estimation toward the high-frequency end of the spectra, octave binning divides the power spectrum into logarithmic frequency bins and calculates the mean and variance of the power spectrum within each bin, thus avoiding any bias between frequencies (for details, see *Fraedrich and Larnder* [1993]). Linear fitting via least squares regression to these bins allows the estimation of α for each scaling range [*Harris et al.*, 1997]. We determined the existence of break points in the spectra by fitting over progressively larger ranges of bins and determining when the addition of the next bin would result in a statistically significant change in the slope of the regression (see Figures 2c, 2d, and 2e). The Fourier transform and linear fitting were applied to the time series of flow, load, and concentration in the LVR data set.

[20] Fourier analysis also offers a direct insight into the question of chemostatic response and L-Q linearity. The Fourier transform of L is given by

$$L(f) = \int_{-\infty}^{\infty} \exp(ift)\mathbf{C} \times Q(t)dt = C_c Q(f), \quad (1)$$

where we have assumed that C_c is a constant (and therefore distinct from C, the time series of concentration). That is,

$$C_c^2 = \frac{|L(f)|^2}{|Q(f)|^2}. \quad (2)$$

If the ratio determined from equation (2) deviates from white noise, then we must reject the hypothesis that C_c is invariant because we will have identified scales over which C_c changes in a self-similar fashion. Such an invalidation does not necessarily imply that these variations in C_c contribute to variation in load to the same extent as variations in Q because this frequency-based analysis does not account for the magnitude of fluctuations. Similarly, white noise scaling in C_c does not necessarily imply that C_c is independent of Q, since the noise in C_c may reflect that in Q [*Feng et al.*, 2004b]. Consequently, analysis of equation (2) is primarily concerned with the identification of time scales on which processes acting against chemostatic behavior might occur.

[21] Spectral analysis in the Little Vermilion River is complicated by the fact that the surface drainage is highly intermittent in comparison to the tile drains, and the tile drains themselves are ephemeral, frequently ceasing to flow in late summer. Although no-flow periods were included in the analysis because the Fourier transform technique requires continuous data, the power spectrum of the flow and concentration is not very sensitive to their presence at subannual time scales. This is because long periods of no flow contribute very little to the local variance of the time series. The presence of no-flow periods does contribute to the signature of annual variability in the flow regimes. Thus, the power spectral representation at subannual time scales can loosely be thought of as representing the hydrological and chemical processes manifested during periods of flow.

2.3.2. Wavelet and Wavelet Coherence Analysis

[22] A wavelet power spectrum (denoted as $|Q^W(f, t)|^2$) can be computed by convolving the time series with a function known as the "mother wavelet" and taking the modulus of the resulting wavelet coefficients. Unlike a Fourier transform, which transforms the entire time series globally, the wavelet transform decomposes the variance of the time series into both frequency and time. By varying the width of the mother wavelet, the contribution of different frequencies to the time series variance may be computed at all points in time over multiple frequency scales (referred to as "dyads") [*Torrence and Compo*, 1998; *Grinsted et al.*, 2004]. Edge effects associated with the convolution of a continuous wavelet and a finite time series reduce the confidence in the computed spectrum near the beginning and end of the time series. This reduction in confidence is most significant at long time scales, resulting in an internal region within which the spectrum is not influenced by the edge effects. The area beyond that region is called the "cone of influence" (COI), where the wavelet spectrum is not reliable. The COI has therefore been excluded from this analysis [*Kumar and Foufoula-Georgiou*, 1997; *Grinsted et al.*, 2004]. The localized wavelet power spectrum can be converted to a global spectrum by averaging over the temporal variability (again excluding the COI). Generally, the global wavelet power spectrum is highly comparable (in at least a qualitative sense) to the power spectrum generated by Fourier analysis and again represents a variance partitioning by frequency.

[23] Because the covariation between power spectra of flow, concentration, and load are of interest, additional techniques are needed to examine correlations between these different spectra. Across all scales we examined such correlations with the wavelet coherence ($R^2(f)$). $R^2(f)$ of time series X and Y is defined as [*Grinsted et al.*, 2004]

$$R^2(f) = \frac{\left|S(f^{-1}XY^w(f)\right|^2)}{S\left(f^{-1}|X^w(f)|^2\right) \cdot S\left(f^{-1}|Y^w(f)|^2\right)}, \quad (3)$$

where S is a smoothing operator (chosen to have a similar footprint as the mother wavelet; here we used a Morlet wavelet) and $XY^w(f)$ is the cross-wavelet spectrum of time series X and Y. The reader is referred to *Grinsted et al.* [2004] for further discussion. The wavelet coherence overall may be interpreted analogously to a correlation coefficient (r^2) between X and Y but in the frequency domain. Again the wavelet coherence can be computed locally or averaged across time in order to produce a global wavelet coherence (GWC). Figures 2f and 2g show the full wavelet spectra of flow and nitrate concentration, respectively, for tile flow station B_1, and Figure 2h shows the wavelet coherence for these two time series.

2.3.3. Relationships in the Time Domain: Multiresolution Analysis

[24] A further use of wavelet techniques in time series analysis is as a mechanism to filter the time series and to isolate contributions at different frequencies. This technique is known as multiresolution analysis (MRA). MRA uses the hierarchical structure of the wavelet transform to isolate contributions to the variance of the full time series at individual dyads (designated level j), providing a time series of fluctuations of level j, referred to as the detailed signature. Mathematically, this is defined as [*Martinez and Amparo Gilabert*, 2009]

$$D_j(t) = \sum_{k=-\infty}^{\infty} W_{j,k}\Psi_{j,k}(t), \quad (4)$$

where $W_{j,k}$ are the wavelet coefficients at dyad j for each time point k and $\Psi_{j,k}$ represents the mother wavelet. By filtering the time series at each dyad j and retrieving the detailed component, a reconstructed time series that contains only fluctuations of period j or greater can be computed from the remainder of the time series. These reconstructed time series are referred to as the approximation time series [*Martinez and Amparo Gilabert*, 2009] and are mathematically defined as

$$A_j(t) = \sum_{k=-\infty}^{\infty} V_{j,k}\Phi_{j,k}(t), \quad (5)$$

where $V_{j,k}$ are the scaling coefficients and $\Phi_{j,k}$ is the father scaling function.

[25] By examining the relationships between the approximation time series of L and Q, we gain detailed insight

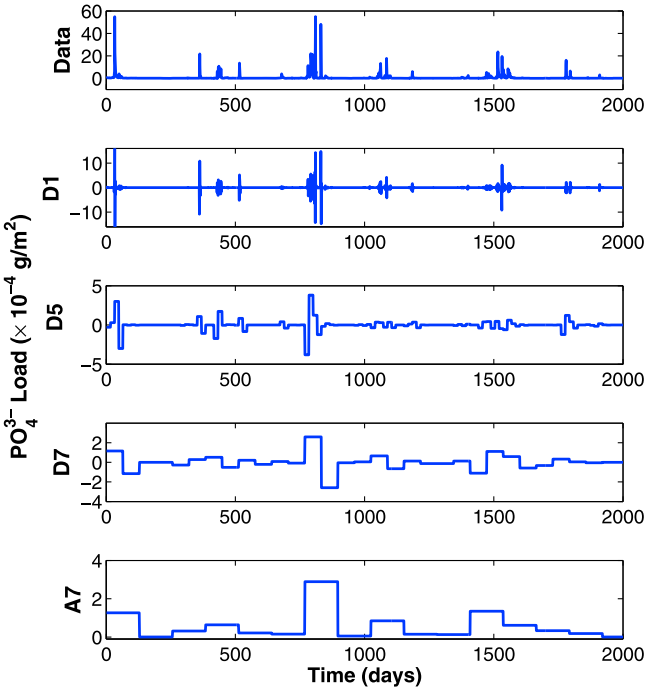

Figure 3. Example of the output of a multiresolution analysis of L (load discharge) for PO_4^{3-}. Plots correspond to (top to bottom) the raw data; the detailed time series computed at levels 1, 5, and 7 (which approximately correspond to daily, monthly, and seasonal time scales); and the approximation (or smoothed) time series computed at seasonal scales.

into the scales of averaging at which a deterministic (linear) L-Q relationship explains most of the variation in L and at which L is thus most predictable. In order to avoid spurious relationships within the correlation analysis, the MRA was undertaken using a Haar wavelet, which does not interpolate between different time points. An example of the approximation and detailed time series generated from the MRA are provided in Figure 3.

2.4. Analyses Undertaken

[26] The specific analyses of the LVR data set undertaken using the techniques in section 2.3 are summarized in Table 2. Fourier spectral analysis was used to examine the scaling properties of the hydrological and biogeochemical signals. Factors affecting chemostatic behavior in L-Q were investigated by (1) examining the ratio of the power spectra of load and discharge, (2) computing the global wavelet coherence (GWC), and (3) calculating the correlation between the approximated time series of L and Q, generated from MRA at interannual time scale.

3. Results and Discussion

3.1. Fourier Spectral Analysis of Precipitation-Normalized Discharge

[27] The scaling exponents α that describe the power spectra of discharge (normalized by precipitation) in each of the surface, tile flow, and river channel stations are presented in Figure 4. The frequencies of the breaks in scale are reported in Table 3. Error bars on each of the points reflect the standard error of the fitted slopes. Two trends emerge strongly: first, the number of scaling regimes that can be identified in the flow signature increases from two in the surface flow stations to three in the tile and river channel stations. Second, the value of the high-frequency scaling exponents also increases from ~0.5 in the surface drains to ~1.25 in the tile drains and ~2 in the river stations. The low-frequency scaling exponents are comparable between all sites and are approximately zero. This white noise signature is the residual signal from rainfall forcing on the system. The midrange and high-frequency exponents increase systematically from tile drain to river channel, indicating increased modification of the flow signature.

[28] We hypothesize that each of the different observed scaling regimes arises from a different set of processes. As a further hypothesis, we consider a multiplicative Fourier domain representation of the scaling in which the power spectrum can be decomposed into the contributions from multiple processes [cf. *Dolgonosov et al.*, 2008]:

$$|Q(f)|^2/|P(f)|^2 \approx \frac{1}{f^{\alpha_1}+\beta_1}\cdot\frac{1}{f^{\alpha_2}+\beta_2}\cdots, \qquad (6)$$

where α_i and β_i are parameters representing the power spectrum of a process that contributes to the overall $|Q(f)|^2/|P(f)|^2$ spectrum. This simple model of multiple-frequency regimes allows us to mathematically link several features of the observed spectra to underlying scaling regimes. First, at sufficiently low frequencies, equation (6) approximates white noise, which can be interpreted as indicating a regime in which all discharge responses reflect rainfall forcing. Assuming $\beta_1 \gg \beta_2$, the transition from power law scaling to white noise occurs at frequencies where $f^{\alpha_1} \sim \beta_1$. The strictest interpretation is that these transitions represent the time scales when the flow path of interest stops contributing noticeably to the variance of the time series. We can therefore interpret $1/\beta_1$ as an estimate of the duration of the pressure wave generating transport in the flow path of interest at any particular spatial scale. The appearance of

Table 2. Analyses Undertaken to Explore L-Q and C-Q Behavior

Analysis	Purpose	Figure or Table
	C and Q Dynamics	
Scaling analysis	scaling regimes	Figure 5
Global wavelet coherence	time scales where C-Q coupling maximized	Figures 6 and 7
	L and Q Dynamics	
Scaling analysis	scaling regimes	Figures 2 and 4
Power spectral ratios	time scales of nonchemostatic processes	Table 3
Global wavelet coherence	time scales that maximize predictability	Figures 2 and 7
MRA approximation time series correlative analysis	time scales that maximize predictability	Figures 3 and 8

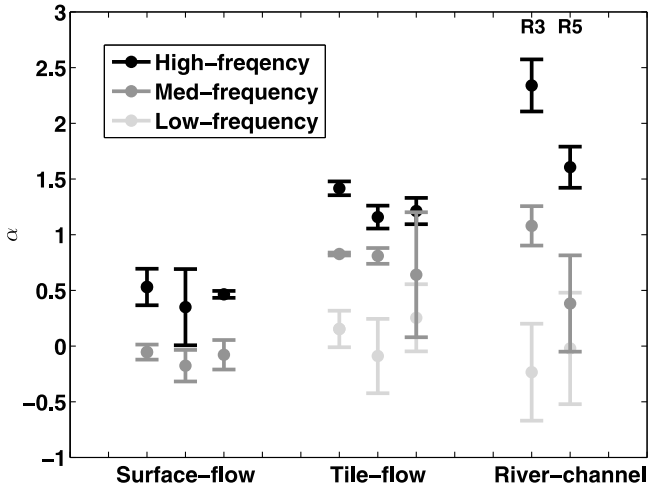

Figure 4. Power law exponents (α) of concentration power spectra for the three chemicals at all sites. Error bars indicate the standard error in the fitted exponents, and scaling breaks are documented in Table 3. The sequence of surface flow is (left to right) A2, B2, and C2 for each chemical and A1, B1, and C1 for tile flow for each chemical.

white noise scaling at relatively high frequencies or low residence times (f = 1/12) in the surface flow stations compared to the tile and rivers (f = 1/120) is consistent with this interpretation. Second, the relative magnitudes of α_1 and α_2 can be computed by calculating the difference ($\Delta\alpha$) in exponents between different scaling regimes (provided that this calculation occurs well away from the breakpoints where mixed terms, e.g., $\beta_2\alpha_1$, contribute strongly to the scaling).

[29] $\Delta\alpha$ between the midfrequency and high-frequency scaling regimes in both the tile drain and the surface flow were both approximately 0.5. That is, the flow processes in the tile drain reflect the same spectral pattern as in the surface drain at high frequencies but contain an additional scaling regime which we attribute to the influence of subsurface processes. Because the surface and subsurface drainage networks are comparable in their extent, it is tempting to attribute the similarity in $\Delta\alpha \sim 0.5$ in each flow station primarily to free surface or pipe flow in the surface and subsurface drainage networks. The appearance of the second scaling regime (medium-low frequencies) in the tile drain would then seem to indicate a process with much slower fluctuations which is presumably related to the time scales at which the water table depth or, equivalently, the volume of the available water storage fluctuates. When comparing the low- to middle-frequency exponents between the tile drain and the river channel, we again compute highly comparable $\Delta\alpha$ values (~0.5–1), which we interpret as being the signature of water table–driven tile flow discharge on the whole watershed [*van der Velde et al.*, 2009]. This is consistent with the known significance of tile drainage as comprising 90% of streamflow in the LVR [*Algoazany*, 2006]. The large $\Delta\alpha$ values associated with the high-frequency river flow regime reflect the much larger area sampled by the river network and the increased storage and travel times in this regime. Thus, R_3 has larger $\Delta\alpha$ than R_5, consistent with its larger drainage area. With one exception, the identification of an intermediate scaling regime was statistically significant (at a 95% confidence level). In all cases, the correspondence between the observed $\Delta\alpha$ values in the different flow regimes remains striking. Consequently, we interpret the spectral signatures observed at each station as reflecting differing degrees of hydrological filtering by the landscape, drainage, and river networks.

3.2. Fourier Spectral Analysis of Concentration Time Series

[30] The scaling exponents α describing the power spectra of concentration for each of the solutes in the surface, tile flow, and river channel stations are presented in Figure 5, and the scale breaks are reported in Table 3.

[31] In many respects the trends in the concentration spectra mirror those in the flow spectra, indicating the importance of flow paths in dictating the concentration dynamics. Again, the lowest exponents arise in the surface drains, where all solutes behave similarly. The influence of subsurface flow is evident in the higher values of α in the tile flow drains. Similarly to Figure 4, the low-frequency river exponents are well approximated by the tile flow exponents. The scale breaks in the concentration spectra are also closely aligned with the middle- to high-frequency scale breaks in the $|Q(f)|^2/|P(f)|^2$ spectra. The greatest difference between the three solutes is a greater α for nitrate in both the tile flow exponents and the low-frequency river-scale exponents when compared to phosphate and atrazine.

Table 3. Frequencies of Break Points for Q/P and C and Lowest Frequency Where $|L(f)|^2/|Q(f)|^2$ Is Well Approximated by White Noise[a]

	Q/P Scale Breaks f				
Flow Path	Low-Middle	Middle-High	Solute	L/Q White Noise f	C Scale Breaks f, Low-High
Surface flow	-	1/12	NO_3^{1-}	1/2	-
			PO_4^{3-}	1/2	-
			Atraz	1/2	-
Tile flow	1/120	1/12	NO_3^{1-}	1/2	-
			PO_4^{3-}	1/64	-
			Atraz	1/64	-
River channel	1/120	1/12	NO_3^{1-}	1/2	1/12
			PO_4^{3-}	1/64	1/23
			Atraz	1/128	1/12

[a]White noise scaling persists from the identified frequency to interannual scale (f = 1/1024). Variation between replicates of each sampling type was low. Where there was disagreement between sites, the lowest frequency at which white noise commenced is presented. Units of f are d^{-1}, and Atraz indicates atrazine.

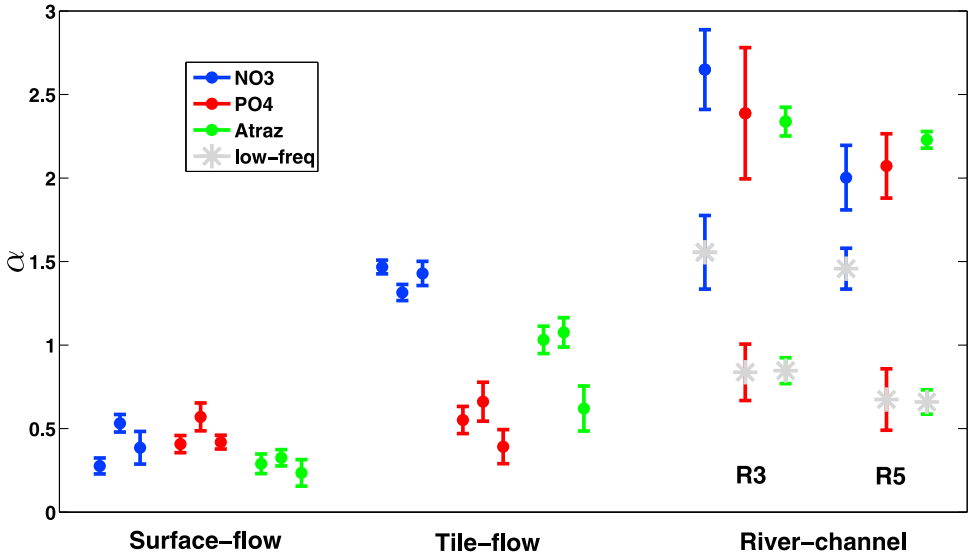

Figure 5. Power law exponents (α) of flow power spectra (normalized by precipitation to isolate the hydrological filter) for the different scaling regimes identified at all sites. The sequence of surface flow is (left to right) A2, B2, and C2, and the sequence for tile flow is A1, B1, and C1. NO3 indicates nitrate, PO4 indicates phosphate, and Atraz indicates atrazine. Error bars indicate the standard error of the fitted exponents. See Table 3 for the location of the scale breaks.

We attribute these differences primarily to the different sorptivities of the chemicals. The appearance of phosphate and atrazine in tile drain flow mostly occurs shortly after application and presumably reflects rapid transport via a network of preferential flow paths in the vadose zone [*Kladivko et al.*, 1999, 2001; *Haws et al.*, 2004, 2005]. Phosphate has the highest sorptivity coefficient of the three chemicals, and its transport is primarily associated with very large flow events (this can be directly verified by consideration of chemograph and hydrograph data and is consistent with the numerical predictions of *McGrath* [2007] that suggest that the relative proportion of export occurring in fast flow pathways scaled with sorption). Under these conditions, preferential macropore flow likely contributes a majority of the flow to the tile drain. The very short residence times (usually ~1 h for 1 m depth flow to tiles [*Haws et al.*, 2004, 2005] associated with macropore flow mean that this flow path has only a weak spectral signature; consequently, flow in the tile network again is the dominant term. This accounts for the strong similarities between phosphate spectra in both surface and tile flow. Note that given the flat topography and similar spatial area drained, residence times in overland flow and the tiles are likely to be similar. In contrast, nitrate has longer residence times in both the saturated and unsaturated zones and, as can again be verified from chemograph and hydrograph data, nitrate is exported in almost all flow events. Plainly, atrazine has a spectral signature that is intermediate between the two cases, and examination of chemograph and hydrograph data indicates that although atrazine is primarily exported during large-flow events, it continues to be mobilized in smaller events where phosphate was largely absent and consequently exhibits an "intermediate" spectral exponent in the tile flow. It appears, therefore, that the tile flow exponents primarily reflect the relative sorption of the three chemicals. Surprisingly, the effect of reactivity and the shorter half-lives of phosphate and atrazine compared to nitrate in the catchment (see high-frequency components of R3 and R5 in Figure 5) do not appear strongly in this signature, again presumably because of the minimal contribution of periods of no export to the variance of the concentration time series.

3.3. Fourier Spectral Analysis of $|L(f)|^2/|Q(f)|^2$ Ratio

[32] As discussed in section 2.3.1, deviations from white noise scaling in the ratio of $|L(f)|^2/|Q(f)|^2$ are indicative of scaling processes that deviate from the chemostatic hypothesis. At long time scales, $|L(f)|^2/|Q(f)|^2$ associated with all hydrological flow paths and all chemical constituents tended toward white noise. However, the smallest time scale at which this white noise regime was encountered varied with the flow path and the solute, as shown in Table 3.

[33] All solutes behaved similarly to each other in the surface stations with the $|L(f)|^2/|Q(f)|^2$ spectra approximating white noise at all scales. This suggests that mobilization is the dominant process contributing to export via surface flow paths, and there are no significant variations in the chemical composition of water transported in this path over different time scales. The white noise scaling regimes were similar for all solutes in the tile and river stations, suggesting that alterations to the chemistry occur primarily in the subsurface flow paths. The nitrate $|L(f)|^2/|Q(f)|^2$ ratio was white noise at almost all locations and scales; that is, nitrate displayed chemostatic behavior everywhere. This reflects two factors: (1) $K_d \sim 0$ for nitrate, meaning that it is highly mobile and that the presence of a large reservoir of nitrogen (which, on the basis of previous studies, is anticipated to consist primarily of organic nitrogen [*Goss et al.*, 1993; *Addiscott*, 1996]) and (2) nitrate is not significantly depleted by the ongoing efflux. Both atrazine and phosphate

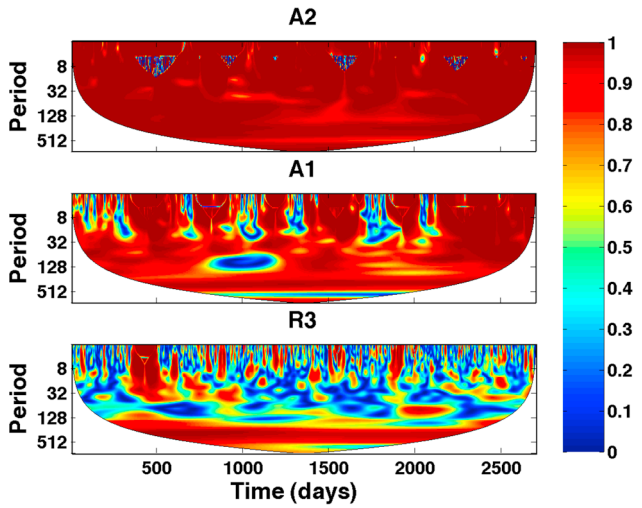

Figure 6. An example of the squared wavelet coherence between the standardized flow and nitrate concentration spectra for three types of sites: (top) a representative surface drain (A_2), (middle) a tile drain (A_1), and (bottom) the lower catchment river station (R_3). Increased complexity and decoupling of discharge and concentration are evident as the spatial scale and dominance of subsurface flow paths increase.

spectra showed distinct power law scaling regimes, indicating time scales over which biogoechemical processes strongly modulate the observed transport behavior and prevent the emergence of chemostatic regimes. The time scales on which the power law scaling regime for atrazine transitioned to white noise (approximately 60 days) corresponds closely to the degradation time scale of atrazine. This scaling regime may therefore reflect the rate of disappearance of atrazine from the system. Reaction time scales are much more difficult to define for P because of its complex biogeochemistry [*Reddy et al.*, 2005], but the spectral signature suggests that an "effective" reaction time scale, also on the order of 60 days, could be hypothesized to describe the immobilization of P in the LVR. An alternative interpretation, however, is that the common 60 day time scale in both cases reflects the typical time scales of crop growth and uptake. Evidently, separating biological uptake from geochemical processes on the basis of stream concentrations alone remains difficult. Overall, however, it appeared that the most mobile of the constituents, nitrate, displayed the most chemostatic behavior.

3.4. Wavelet Coherence Analysis of *L*-*Q* and *C*-*Q*

[34] Wavelet coherence can be interpreted analogously to a Pearson's correlation coefficient in the frequency domain (see details in section 2.3.2 and Figure 7) and can be used to identify if processes occurring at a particular time scale generate the same responses in two different signals. Loosely, this can be interpreted as the strength of coupling between two different signals over a range of frequencies. Figure 6 gives examples of the wavelet coherence of flow and nitrate concentration for each of the three types of sites, showing a progressive decoupling of flow and concentration from surface drains to tile drains and the river station. Global wavelet coherence (GWC) plots for the exported load and concentration of each solute at each scale are presented in Figure 7. The GWC differs with the flow path and with solute type. In the surface flow stations a strong coupling between discharge and concentration and discharge and load was found for all solutes. At within-year time scales, tile flow stations showed a lower degree of coupling than the surface stations but a stronger coupling than in the river channel. This was particularly exaggerated in the concentration discharge GWC. However, at annual or longer scales, the coupling between load discharge and concentration discharge in the river stations increased.

[35] The wavelet coherence plots suggest several features of the coupling between flow and biogeochemistry. However, caution is needed when interpreting this "coupling" between two time series because the wavelet coherence reflects the timing of fluctuations but not necessarily their magnitude. Consequently, we see a significant coherence between flow and load at all time scales (Figure 7a) because load is a function of flow. Conversely, high coherence between discharge and concentration only emerges at annual time scales (Figure 7b), reflecting the dominant annual anthropogenic forcing associated with fertilizer and pesticide application. The fact that the strongest phosphate-flow coupling arose not at the annual but at longer time scales is reflected in the recorded fertilization dates for the LVR. Phosphate has more irregular fertilizing timing compared to nitrate and atrazine, both of which have regular annual cycles of application.

3.5. Multiresolution Analysis of *L*-*Q*

[36] We examined patterns in the r^2 values for a linear regression between L and Q evaluated on each dyadic level of the approximation time series generated from the MRA (see Figure 3). Across the majority of the sites and chemical species we found that the r^2 peaked at the dyadic level associated with variation on 128–255 day time scales. The approximation time series at this level preserves variation on seasonal and greater time scales (time scales which resolve variations in chemical application and the annual cropping cycles) but smooths over within-season variation. The r^2 values generated at this smoothing level for the linear L-Q regression across all chemical species and sites are presented in Figure 8. The surface drainage r^2 values were highly variable, while the tile flow and river channel sites were more consistent both across sites and between the river and tile stations. Nitrate displayed high r^2 values at all stations, while the r^2 values of L-Q for atrazine and phosphate declined from surface flow stations to tile and river stations.

[37] The highly variable L-Q r^2 in the three surface drains is difficult to explain and presumably reflects site-to-site differences (e.g., in local topography, drain design, crops, and agricultural practices and the resulting availability of the phosphate sources). The minimal differences in the r^2 behavior at tile and river stations appear to be consistent with the similarities in the scaling behavior of C and Q in tile and river stations at low frequencies as shown in Figures 4 and 5. The primary deviations in transport processes between these systems were associated with high frequencies, which are essentially removed by the wavelet filtering. The large

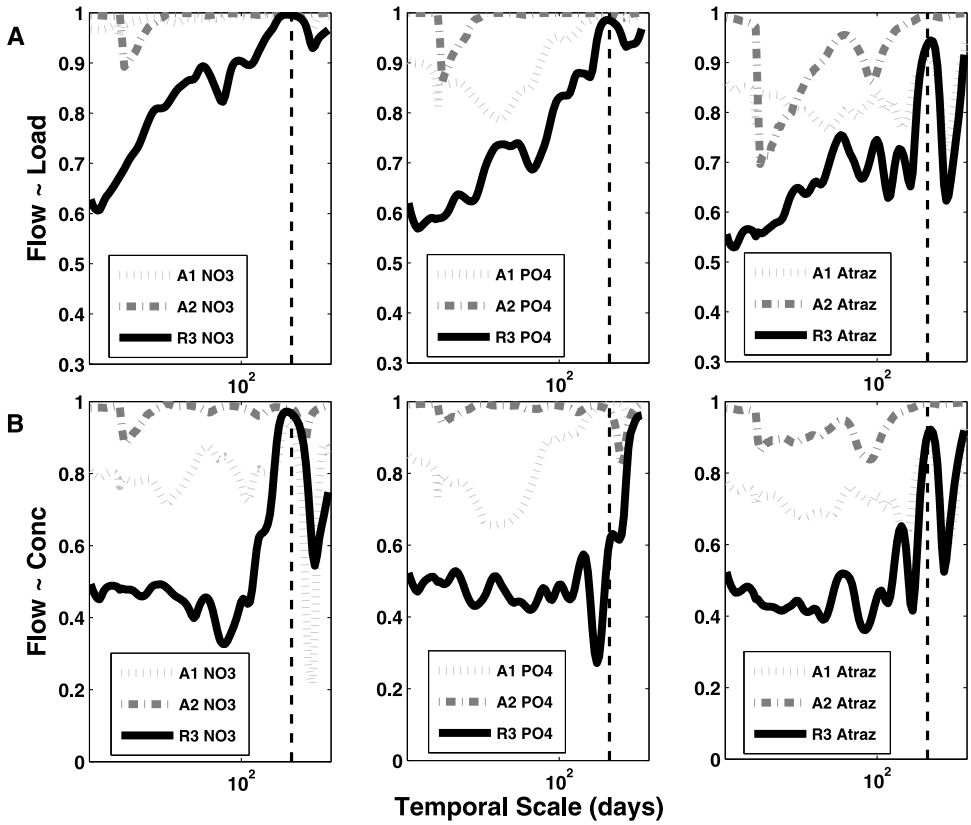

Figure 7. Global squared wavelet coherence (a) between flow and load and (b) between flow and concentration, computed as the average across the temporal variability at each frequency (excluding edge effects region COI). The dashed line identifies the annual frequency. NO3 indicates nitrate, PO4 indicates phosphate, and Atraz indicates atrazine.

declines in phosphate and atrazine L-Q r^2 in tile and river stations versus surface stations reflect the importance of subsurface biogeochemical processes in altering the availability and mobility of these chemicals, consistent with the observations in Table 3. These results indicate that there is a distinct difference in the degree of chemostatic response observed for the three chemical species at the interannual scale, with nitrate being the most "chemostatic" and atrazine the least.

4. Summary and Conclusions

[38] This study was motivated by three key questions: (1) How do concentration and flow scale in the frequency

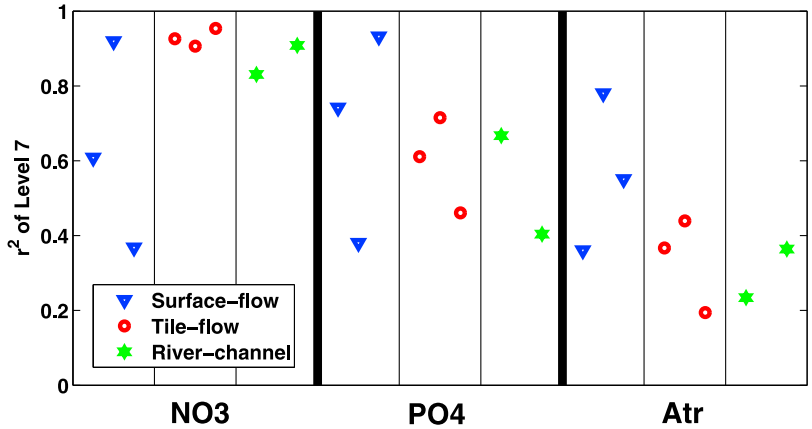

Figure 8. Pearson's correlation coefficient (r^2) between filtered L and Q time series based on the seasonal approximation (level 7) from the MRA for all sites and chemicals. The symbol sequence for each chemical is (left to right) A2, B2, C2, A1, B1, C1, R3, and R5. NO3 indicates nitrate, PO4 indicates phosphate, and Atr indicates atrazine.

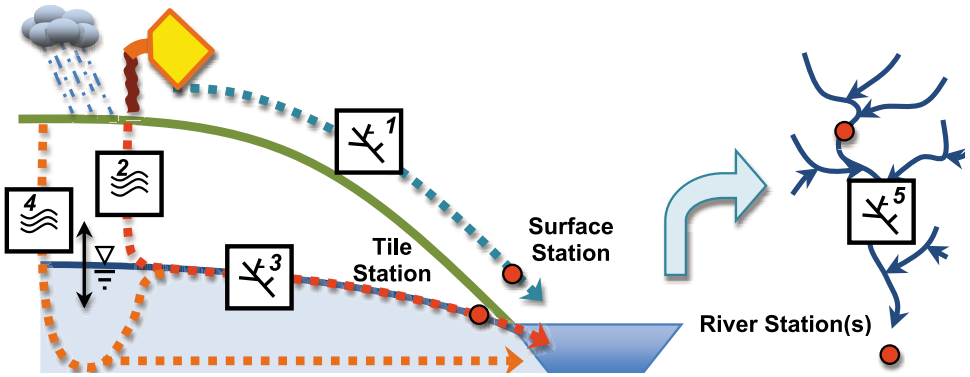

Figure 9. The multiple flow paths and filters in the catchment. Red circles indicate the location of sampling points relative to the flow paths. Network–surface flow "filters" (1, 3, and 5) are present in the surface drainage networks, the tile drain network, and the river network. The properties of these filters vary with scale and with network structure. The vadose zone provides additional filtering (filter 2), which is likely to be stronger for matrix flow and weaker for macropore flow. Vadose zone–water table flow paths (filter 4) provide longer residence times, driven by the time scales of water table response, and, consequently, the greatest potential for transformation of chemical and hydrological signals. Although 90% of flow in the catchment follows the tile drains, there is potential for the water table to discharge directly to the channels. We do not sample this flow path directly, but its contribution to the river channel is sampled in the river stations. Chemical filtering in filters 2 and 4 is driven by hydrological transport and chemical availability in these zones. Chemical availability is a function of renewal and removal from transport. The effect of these filters in series is multiplicative and contributes to the appearance of multiple scaling regimes in the Fourier domain.

domain (as metrics of filtering)? (2) Does the observed scaling behavior "fingerprint" different reactive transport processes? (3) On what spatial and temporal scales are chemostatic responses observed for the three chemicals considered? We can now answer these questions explicitly on the basis of the analysis in this paper. It must be recognized, however, that process diagnosis based on time series analysis alone is not definitive but rather forms the basis for a conceptual model of solute filtering in the catchment. More explicit verification of the interpretations offered in this section is necessary and is discussed in section 4.5. However, for clarity, an illustration of the conceptual model of hydrological and biogeochemical filtering in the catchment that emerges from the frequency-based analysis is presented in Figure 9 and is referred to throughout this discussion.

4.1. How Do Concentration and Flow Scale?

[39] Concentration and flow-scaling regimes showed strong parallels. The major trend in the scaling exponents for both solute concentration and the normalized flow (see Figures 4 and 5) was the increase across hydrologic flow paths and spatial scales from surface drain to the tile flow stations, with further increases in the river stations. This trend can be broadly linked to increased catchment residence times at each scale, and process relationships to the scaling regimes may be inferred by considering the breaks in scaling and the response of different solutes. Specifically, it appears that the highest-frequency scaling regimes in R3 and R5 relate to tile or surface flow in the networks: either the surface drain network (Figure 9, filter 1), the tile drain network (filter 3), or the river network (filter 5). The similarities in discharge $\Delta\alpha$ associated with the low-frequency to midfrequency scaling regimes for Q in the tile stations and the river channels, along with the absence of an intermediate scaling regime in the surface flow case, strongly suggest that this frequency range is dominated by slower modulations of the water table and consequently by the storage capacity in the soil (Figure 9, filters 2 and 4). The clear emergence of three scaling regimes in the stream discharge suggests that time scales of transport in a diversity of runoff pathways in agricultural catchments may be inferred on the basis of flow data from the streams alone. Filtering flow and concentration time series at scales that correspond to these different regimes may even allow estimates of the mass contribution associated with these distinct flow paths to be made on the basis of in-stream concentrations, offering a complementary approach to requiring explicit observation of all contributions in the catchment [cf. *Rozemeijer et al.*, 2010a].

4.2. Can We Identify Reactive Transport Processes?

[40] By linking the scaling regimes of discharge and concentration, we argue that signatures of reactive transport processes and pathways can be inferred. Although phosphate, atrazine, and nitrate are all exported by the tile drains, much larger scaling exponents are associated with nitrate compared to phosphate or atrazine in the tile drains and the low-frequency regime of the river stations. We interpret this observation by suggesting that these scaling regimes are associated with primarily a vadose zone–macropore flow path for phosphate and atrazine (Figure 9, filter 2) but with a vadose zone–saturated zone flow path for nitrate (Figure 9, filter 4). This is consistent with the higher application rates of nitrate compared to atrazine and phosphate, resulting in larger concentrations and residence times of nitrate in the

subsurface, and with the importance of surface chemistry in retaining P and atrazine in the soil matrix and thus favoring transport in macropores [*Haws et al.*, 2004]. Thus, the different scaling behavior of nitrate in the tile and river stations appears to act as a fingerprint both of the location of mobile stores of the different chemicals (soil surface or vadose zone dominated for phosphate and atrazine, vadose zone or water table dominated for nitrate) and of the different transport pathways that control mobilization of the solutes (Figure 9, filters 2 and 4).

[41] This interpretation also appears consistent with the analysis of $|L(f)|^2/|Q(f)|^2$ for the different solutes. If long-term reservoirs of nitrate are present in the subsurface, then export of nitrate may be primarily driven by transport processes so that the approximation of $|L(f)|^2/|Q(f)|^2$ as white noise at all scales is reasonable. In contrast, the export behavior of atrazine and phosphate is modified by the time scales of removal (geochemically or due to plant uptake) and also potentially by dilution processes (e.g., between macropore flow and water table contributions) in the tile drains. The emergence of scaling behavior in $|L(f)|^2/|Q(f)|^2$ may reflect biological, chemical, and mixing processes. Note, however, that the absence of deviations from white noise scaling in the $|L(f)|^2/|Q(f)|^2$ ratio does not imply the absence of removal processes but merely that these removal processes do not alter the variance partitioning in the concentration signal. To resolve this ambiguity, spectral analysis could be complemented by mass balance approaches to offer deeper insight into reactive transport.

[42] The concentration scaling regimes in the river channel appeared invariant with scale for phosphate and atrazine but were scale dependent for nitrate. This suggests that time scales of removal of phosphate and atrazine are either much larger or much smaller than the residence times at R_5 (the upper catchment river station). Indeed, atrazine removal rates from surface waters are almost negligible [*Capel and Larson*, 2001]. Conversely, the higher $\Delta\alpha$ for nitrate at R_5 (~0.75) than R_3 (~1.25) suggests that in-channel processing or removal became more significant with increasing scale, potentially reflecting the greater residence time in the system.

4.3. When Does Chemostatic Behavior Occur?

[43] Chemostatic behavior was most prevalent in the Little Vermilion River Watershed on seasonal to annual time scales and for chemicals where the rate of removal from transport was comparable to or slower than the time scales of chemical renewal. The former condition reflects the importance of annual or interannual applications of chemicals in controlling the mass of solute available for export (and was reflected by, e.g., the strong coherence in the C-Q and L-Q wavelet coherence at annual time scales). The latter condition allows a pseudosteady concentration of mobile solute to persist in subsurface reservoirs. Export from the subsurface is sensitive to the availability of water to drive transport; thus, loads respond strongly to variation in flow.

[44] In the Little Vermilion River Watershed, chemostatic behavior arises from the combination of human modification of hydrological flow paths and human amendment of the biogeochemical regime through regular addition of agrochemicals. The addition of fertilizers or pesticides is large in comparison to the capacity of natural biogeochemical processes to cycle and remove these chemicals from the system. This leads to a minimal influence of biogeochemical cycling on the resulting chemical export in comparison to anthropogenic forcing. This allows for accumulation of nutrient stores in soils, which is the manifestation of intensive management over the past several decades. Similarly, the modification of the hydrology reduces both the mean and the variance of residence times in the catchment, preventing hydrological complexity from obscuring the chemostatic signals.

4.4. Implications for Environmental Management

[45] Limited in-stream processing and the resulting emergence of near-linear load-flow relationships are well established at large scales in the Mississippi-Missouri River Basin [*Basu et al.*, 2010a]. The analysis presented here demonstrates that such behavior is also characteristic of export at the smallest scales (tile and surface drainage areas) contributing flow and chemicals to the river systems. That is, anthropogenic impacts appear to override natural biogeochemical processing at all spatial scales in the basin.

4.5. Broader Implications and Future Work

[46] The simplicity of hydrological pathways in the Little Vermilion River Watershed allowed us to inferentially link the observed discharge, load, and concentration scaling regimes to hydrological and chemical processes. There may be potential to use similar observations of scaling regimes to learn about runoff pathways in more complex catchments, if the observed scaling regimes can be unambiguously linked to different runoff generation mechanisms. In larger, more complex catchment systems, similar scaling regimes in streamflow are known to arise [*Milly and Wetherald*, 2002; *Dolgonosov et al.*, 2008]. Previously, authors have tended to relate the observed scaling regimes to bulk representations of catchment reservoir models [*Milly and Wetherald*, 2002], attributing the break in scale at weekly to monthly time scales to spatial variation in rainfall [*Dolgonosov et al.*, 2008]. This study has highlighted the potential for the different scaling regimes to reflect runoff regimes associated primarily with fast flow generation processes and with the slower modulations of base flow by changes in water table depth [*Zhang and Schilling*, 2004]. It is intriguing to speculate that, at least in these agricultural settings, the breaks in scaling could be used to develop appropriate windows to use for hydrograph separation. *Wörman et al.* [2010] have shown that systematic changes in the spectral properties of streamflow over time may be links to human impacts such as stream damming and land use change, suggesting that scaling exponents may also have a role as indicators of hydrological and catchment-scale change.

[47] The conceptual model developed from inference based on the frequency domain analysis here is not definitive, and further verification is needed. One approach for such verification is to develop process-based models of hydrological and biogeochemical response in tile-drained agricultural catchments that could represent the different processes associated with nitrate, phosphate, and atrazine mobilization. In particular, spatial and temporal intermittency in the application of pesticides and fertilizers between

different farms in the catchment leads to spatiotemporal variability in the forcing on the catchment. The implications of this variation for the emerging spectral signatures of concentration are not well defined and could not be definitively isolated within the Little Vermillion River Watershed data set. The precise translation of this variability into the properties of the power spectra of export requires further investigation to assist in the robust interpretation of concentration data at large spatial scales. Convergence of the patterns of export predicted by such process-based models to observations in the LVR would provide additional verification of the conceptual model. The Fourier and wavelet spectra and the multiresolution signatures of hydrology and biogeochemistry in the catchment provide excellent targets for model validation. Similarly, frequency-based tools in either the Fourier or wavelet domain offer alternative approaches for model diagnostics, which complement diagnostics purely on the basis of matching time series [*Siqueira et al.*, 2006; *Mahecha et al.*, 2010; *Schaefli and Zehe*, 2009]. Time domain validation is biased toward identifying the processes which contribute most of the variance over the length of the simulation. By contrast, frequency domain validation identifies scales where a model performs poorly, potentially helping to identify missing processes or knowledge gaps.

[48] Conceptualizing catchments as filters originally offered new perspectives on time series analysis and the propagation of rainfall into surface and subsurface runoff. It appears that at least in simple systems it is possible to link the characteristics of the resulting scaling regimes to identifiable physical processes that take place within the catchments, allowing the filter concept to be linked to mechanistic understanding of rainfall-runoff response. More fundamentally, however, the filter concept appears to have new applicability as catchments are increasingly visualized as complex systems in which biogeochemical and ecological processes respond to rainfall and streamflow drivers. As high-resolution concentration and flow data sets become available from a wider range of sites, the biogeochemical aspects of this filtering can be explored further. Expanding the filter concept of catchments to ecological processes, with their many complex drivers, remains an important frontier for future work.

[49] **Acknowledgments.** This study was conducted as part of the NSF-funded hydrologic synthesis project Water Cycle Dynamics in a Changing Environment: Advancing Hydrologic Science through Synthesis (NSF grant EAR-0636043, M. Sivapalan, PI). We thank Anders Wörman for constructive comments on the manuscript.

References

Addiscott, T. (1996), Fertilizers and nitrate leaching, in *Agricultural Chemicals and the Environment, Issues in Environmental Science and Technology*, vol. 5, pp. 1–26, R. Soc. of Chem., Cambridge, U. K.

Algoazany, A. (2006), Long-term effects of agricultural chemicals and management practices on water quality in a subsurface drained watershed, Ph.D. thesis, Univ. of Ill. at Urbana-Champaign, Urbana.

Basu, N. B., P. S. C. Rao, E. H. Winzeler, S. Kumar, P. R. Owens, and V. Merwade (2010a), Identification of dominant controls on hydrologic responses in engineered watersheds: 1. Hydrograph prediction, *Water Resour. Res.*, *46*, W04501, doi:10.1029/2009WR007803.

Basu, N. B., et al. (2010b), Nutrient loads exported from managed catchments reveal emergent biogeochemical stationarity, *Geophys. Res. Lett.*, *37*, L23404, doi:10.1029/2010GL045168.

Blann, K., J. Anderson, G. Sands, and B. Vondracek (2009), Effect of agricultural drainage on aquatic ecosystems: A review, *Crit. Rev. Environ. Sci. Technol.*, *39*(11), 909–1001.

Borsuk, M., C. Stow, and K. Reckhow (2004), Confounding effect of flow on estuarine response to nitrogen loading, *J. Environ. Eng.*, *130*(6), 605–614, doi:10.1061/(ASCE)0733-9372.

Botter, G., E. Bertuzzo, and A. Rinaldo (2010), Transport in the hydrologic response: Travel time distributions, soil moisture dynamics, and the old water paradox, *Water Resour. Res.*, *46*, W03514, doi:10.1029/2009WR008371.

Brusseau, M. L., and P. S. C. Rao (1989), Sorption nonideality during organic contaminant transport in porous media, *Crit. Rev. Environ. Sci.*, *19*(1), 33–99.

Capel, P., and S. Larson (2001), Effect of scale on the behavior of atrazine in surface waters, *Environ. Sci. Technol.*, *35*(4), 648–657, doi:10.1021/es001220f.

Cardenas, M. B. (2008), Surface water-groundwater interface geomorphology leads to scaling of residence times, *Geophys. Res. Lett.*, *35*, L08402, doi:10.1029/2008GL033753.

Dolgonosov, B., K. Korchagin, and N. Kirpichnikova (2008), Modeling of annual oscillations and 1/*f*-noise of daily river discharges, *J. Hydrol.*, *357*(3–4), 174–187, doi:10.1016/j.jhydrol.2008.04.023.

Evans, R. O., and N. R. Fausey (1999), Effects of inadequate drainage on crop growth and yield, in *Agricultural Drainage*, vol. 1, pp. 13–54, Am. Soc. of Agron., Madison, Wis.

Feng, X., J. W. Kirchner, and C. Neal (2004a), Measuring catchment-scale chemical retardation using spectral analysis of reactive and passive chemical tracer time series, *J. Hydrol.*, *292*(1–4), 296–307, doi:10.1016/j.jhydrol.2004.01.012.

Feng, X., J. W. Kirchner, and C. Neal (2004b), Spectral analysis of chemical time series from long-term catchment monitoring studies: Hydrochemical insights and data requirements, *Water Air Soil Pollut. Focus*, *4*(2–3), 221–235, doi:10.1023/B:WAFO.0000028356.24722.b1.

Fraedrich, K., and C. Larnder (1993), Scaling regimes of composite rainfall time series, *Tellus, Ser. A*, *45*, 289–298.

Godsey, S., J. Kirchner, and D. Clow (2009), Concentration-discharge relationships reflect chemostatic characteristics of US catchments, *Hydrol. Processes*, *23*, 1844–1864.

Godsey, S. E., et al. (2010), Generality of fractal 1/*f* scaling in catchment tracer time series, and its implications for catchment travel time distributions, *Hydrol. Processes*, *24*, doi:10.1002/hyp.7677.

Goss, M., K. Howse, P. Lane, D. Christian, and G. Harris (1993), Losses of nitrate-nitrogen in water draining from under autumn sown crops established by direct drilling or moldboard plowing, *J. Soil Sci.*, *44*(1), 35–48.

Grinsted, A., S. Jevrejeva, and J. Moore (2004), Application of the cross-wavelet transform and wavelet coherence to geophysical time series, *Nonlinear Processes Geophys.*, *11*, 561–566, doi:10.5194/npg-11-561-2004.

Harris, D., A. Seed, M. Menabde, and G. Austin (1997), Factors affecting multiscaling analysis of rainfall time series, *Nonlinear Processes Geophys.*, *4*, 137–156.

Haws, N. W., B. S. Das, and P. S. C. Rao (2004), Dual-domain solute transfer and transport processes: Evaluation in batch and transport experiments, *J. Contam. Hydrol.*, *75*(3–4), 257–280, doi:10.1016/j.jconhyd.2004.07.001.

Haws, N. W., P. S. C. Rao, J. Simunek, and I. C. Poyer (2005), Single-porosity and dual-porosity modeling of water flow and solute transport in subsurface-drained fields using effective field-scale parameters, *J. Hydrol.*, *313*(3–4), 257–273, doi:10.1016/j.jhydrol.2005.03.035.

Katul, G. G., A. Porporato, E. Daly, A. C. Oishi, H.-S. Kim, P. C. Stoy, J.-Y. Juang, and M. B. Siqueira (2007), On the spectrum of soil moisture from hourly to interannual scales, *Water Resour. Res.*, *43*, W05428, doi:10.1029/2006WR005356.

Kirchner, J. W. (2009), Catchments as simple dynamical systems: Catchment characterization, rainfall-runoff modeling, and doing hydrology backward, *Water Resour. Res.*, *45*, W02429, doi:10.1029/2008WR006912.

Kirchner, J., X. Feng, and C. Neal (2000), Fractal stream chemistry and its implications for contaminant transport, *Nature*, *403*(6769), 524–527.

Kirchner, J., X. Feng, and C. Neal (2001), Catchment-scale advection and dispersion as a mechanism for fractal scaling in stream tracer concentrations, *J. Hydrol.*, *254*(1–4), 82–101.

Kirchner, J., X. Feng, C. Neal, and A. Robson (2004), The fine structure of water-quality dynamics: The (high-frequency) wave of the future, *Hydrol. Processes*, *18*, 1353–1359, doi:10.1002/hyp.5537.

Kladivko, E. J., J. Grochulska, R. F. Turco, G. Van Scoyoc, and J. D. Eigel (1999), Pesticide and nitrate transport into subsurface tile drains of different spacing, *J. Environ. Qual.*, *28*, 997–1004.

Kladivko, E., L. C. Brown, and J. L. Baker (2001), Pesticide transport to subsurface tile drains in humid regions of North America, *Crit. Rev. Environ. Sci. Technol.*, *31*, 1–62.

Kumar, P., and E. Foufoula-Georgiou (1997), Wavelet analysis for geophysical applications, *Rev. Geophys.*, *35*(4), 385–412.

Li, Z., and Y.-K. Zhang (2007), Quantifying fractal dynamics of groundwater systems with detrended fluctuation analysis, *J. Hydrol.*, *336*(1–2), 139–146, doi:10.1016/j.jhydrol.2006.12.017.

Machesky, M., T. Holm, and J. Slowikowski (2010), Phosphorus speciation in stream bed sediments from an agricultural watershed: Solid-phase associations and sorption behavior, *Aquat. Geochem.*, *16*, 639–662, doi:10.1007/s10498-010-9103-2.

Mahecha, M., et al. (2010), Comparing observations and process based simulations of biosphere-atmosphere exchanges on multiple timescales, *J. Geophys. Res.*, *115*, G02003, doi:10.1029/2009JG001016.

Majone, B., A. Bellin, and A. Borsato (2004), Runoff generation and contaminant transport in karst catchments, *J. Hydrol.*, *294*(176–195), doi:10.1016/j.jhydrol.2003.11.042.

Majone, B., A. Bertagnoli, and A. Bellin (2010), A non-linear runoff generation model in small alpine catchments, *J. Hydrol.*, *385*(1–4), doi:10.1016/j.jhydrol.2003.11.042.

Martinez, B., and M. Amparo Gilabert (2009), Vegetation dynamics from NDVI time series analysis using the wavelet transform, *Remote Sens. Environ.*, *113*(9), 1823–1842, doi:10.1016/j.rse.2009.04.016.

Matsoukas, C., S. Islam, and I. Rodriguez-Iturbe (2000), Detrended fluctuation analysis of rainfall and streamflow time series, *J. Geophys. Res.*, *105*(D23), 29,165–29,172.

McGrath, G. (2007), An exploration of the rainfall controls on pesticide transport via fast flow pathways, unpublished Ph.D. thesis, Sch. of Earth and Geogr. Sci., Univ. of West. Aust., Perth, Australia.

McLaughlin, A., and P. Mineau (1995), The impact of agricultural practices on biodiversity, *Agric. Ecosyst. Environ.*, *55*(3), 201–212.

Meng, H., J. Salas, T. Green, and L. Ahuja (2006), Scaling analysis of space-time infiltration based on the universal multifractal model, *J. Hydrol.*, *322*(1–4), 220–235, doi:10.1016/j.jhydrol.2005.03.016.

Milly, P. C. D., and R. T. Wetherald (2002), Macroscale water fluxes: 3. Effects of land processes on variability of monthly river discharge, *Water Resour. Res.*, *38*(11), 1235, doi:10.1029/2001WR000761.

Mitchell, J., G. McIsaac, S. Walker, and M. Hirschi (2000), Nitrate in river and subsurface drainage flows from an east central Illinois watershed, *Trans. ASAE*, *43*(2), 337–342.

Phillips, B., B. Anderson, J. Hunt, S. Huntley, R. Tjeerdema, N. Kapellas, and K. Worcester (2006), Soil-phase sediment toxicity identification evaluation in an agricultural stream, *Environ. Toxicol. Chem.*, *25*(6), 1671–1676.

Rabalais, N., R. Turner, and W. Wiseman (2002), Gulf of Mexico hypoxia, aka "The Dead Zone", *Annu. Rev. Ecol. System.*, *33*, 235–263, doi:10.1146/annurev.ecolsys.33.010802.150513.

Reddy, K. R., R. G. Wetzel, and R. Kadlec (2005), Biogeochemistry of phosphorus in wetlands, in *Phosphorus: Agriculture and the Environment*, edited by J. T. Sims and A. N. Sharpley, pp. 263–316, Soil Sci. Soc. of Am., Madison, Wis.

Rozemeijer, J. C., Y. van der Velde, R. G. McLaren, F. C. van Geer, H. P. Broers, and M. F. P. Bierkens (2010a), Integrated modeling of groundwater-surface water interactions in a tile-drained agricultural field: The importance of directly measured flow route contributions, *Water Resour. Res.*, *46*, W11537, doi:10.1029/2010WR009155.

Rozemeijer, J. C., Y. van der Velde, F. C. van Geer, G. De Rooij, P. J. J. F. Torfs, and H. P. Broers (2010b), Improving load estimates for NO_3 and P in surface waters by characterizing the concentration response to rainfall events, *Environ. Sci. Technol.*, *44*(16), 6305–6312.

Sauquet, E., M.-H. Ramos, L. Chapel, and P. Bernardara (2008), Streamflow scaling properties: investigating characteristic scales from different statistical approaches, *Hydrol. Processes*, *22*, 3462–3475, doi:10.1002/hyp.6952.

Schaefli, B., and E. Zehe (2009), Hydrological model performance and parameter estimation in the wavelet domain, *Hydrol. Earth Syst. Sci.*, *13*, 1921–1936.

Schertzer, D., P. Bernardara, A. Biaou, I. Tchiguirinskaia, M. Lang, E. Sauquet, H. Bendjoudi, P. Hubert, S. Lovejoy, and J. M. Veysseire (2006), Extremes and multifractals in hydrology: Results, validations and prospects, *Houille Blanche*, *5*, 112–119, doi:10.1051/lhb:2006095.

Schilling, K., and M. Helmers (2008), Effect of subsurface drainage tiles on streamflow in Iowa agricultural watersheds: Exploratory hydrograph analysis, *Hydrol. Processes*, *22*, 4497–4506.

Siqueira, M., G. Katul, D. Sampson, P. Stoy, J.-Y. Juang, H. McCarthy, and R. Oren (2006), Multiscale model intercomparisons of CO_2 and H_2O exchange rates in a maturing southeastern US pine forest, *Global Change Biology*, *12*, 1189–1207, doi:10.111/j.1365-2486.2006.01,158.x.

Tessier, Y., S. Lovejoy, P. Hubert, D. Schertzer, and S. Pecknold (1996), Multifractal analysis and modeling of rainfall and river flows and scaling, causal transfer functions, *J. Geophys. Res.*, *101*(D21), 26,427–26,440.

Torrence, C., and G. Compo (1998), A practical guide to wavelet analysis, *Bull. Am. Meteorol. Soc.*, *79*(1), 61–78.

van der Velde, Y., G. G. de Rooj, and P. J. J. F. Trofs (2009), Catchment-scale non-linear groundwater-surface water interactions in densely drained lowland catchments, *Hydrol. Earth Syst. Sci.*, *13*, 1867–1885.

Wauchope, R. D., T. M. Buttler, A. G. Hornsby, P. W. M. Augustijn-Beckers, and J. P. Burt (1992), The SCS/ARS/CES pesticide properties database for environmental decision-making, in *Reviews of Environmental Contamination and Toxicology*, vol. 123, edited by G. Ware, pp. 1–155, Springer, New York.

Wörman, A., G. Lindstrom, A. Akesson, and J. Riml (2010), Drifting runoff periodicity during the 20th century due to changing surface water volume, *Hydrol. Processes*, *24*, 3772–3784, doi:10.1002/hyp.7810.

Zhang, Y., and K. Schilling (2004), Temporal scaling of hydraulic head and river base flow and its implication for groundwater recharge, *Water Resour. Res.*, *40*, W03504, doi:10.1029/2003WR002094.

Zhang, Y., and K. Schilling (2005), Temporal variations and scaling of streamflow and baseflow and their nitrate-nitrogen concentrations and loads, *Adv. Water Resour.*, *28*(7), 701–710, doi:10.1016/j.adwatres.2004.12.014.

Zhou, X., N. Persaud, H. Wang, and H. Lin (2006), Multifractal scaling of daily runoff time series in agricultural watersheds, *J. Am. Water Resour. Assoc.*, *42*(6), 1659–1670.

N. B. Basu, Department of Civil Engineering, University of Iowa, Iowa City, IA 52317, USA. (nandita-basu@uiowa.edu)

K. Guan, Department of Civil and Environmental Engineering, Princeton University, Princeton, NJ 08544, USA. (kguan@princeton.edu)

C. J. Harman, Department of Civil and Environmental Engineering, University of Illinois at Urbana-Champaign, Urbana, IL 61801-2352, USA. (charman2@illinois.edu)

P. K. Kalita, Department of Agricultural and Biological Engineering, University of Illinois at Urbana-Champaign, Urbana, IL 61801, USA. (pkalita@illinois.edu)

A. I. Packman, Department of Civil Engineering, Northwestern University, Evanston, IL 60208-3109, USA. (a-packman@northwestern.edu)

P. S. C. Rao, School of Civil and Environmental Engineering, Purdue University, West Lafayette, IN 47907, USA. (pscr@purdue.edu)

S. E. Thompson, Nicholas School of the Environment, Duke University, Durham, NC 27707, USA. (set8@duke.edu)

M. Sivapalan, Department of Civil and Environmental Engineering, University of Illinois at Urbana-Champaign, Urbana, IL 61801, USA. (sivapala@illinois.edu)